



HAL
open science

Kinetic Analysis of Tropical Lignocellulosic Agrowaste Pyrolysis

Lina Maria Romero Millan, Fabio Emiro Sierra Vargas, Ange Nzihou

► **To cite this version:**

Lina Maria Romero Millan, Fabio Emiro Sierra Vargas, Ange Nzihou. Kinetic Analysis of Tropical Lignocellulosic Agrowaste Pyrolysis. *BIOENERGY RESEARCH*, 2017, 10 (3), pp.832-845. 10.1007/s12155-017-9844-5 . hal-01581811

HAL Id: hal-01581811

<https://imt-mines-albi.hal.science/hal-01581811>

Submitted on 7 Nov 2019

HAL is a multi-disciplinary open access archive for the deposit and dissemination of scientific research documents, whether they are published or not. The documents may come from teaching and research institutions in France or abroad, or from public or private research centers.

L'archive ouverte pluridisciplinaire **HAL**, est destinée au dépôt et à la diffusion de documents scientifiques de niveau recherche, publiés ou non, émanant des établissements d'enseignement et de recherche français ou étrangers, des laboratoires publics ou privés.

Kinetic Analysis of Tropical Lignocellulosic Agrowaste Pyrolysis

Lina María Romero Millán^{1,2}  · Fabio Emiro Sierra Vargas¹ · Ange Nzihou²

Abstract The thermal behavior of three Colombian agricultural residues was studied by non-isothermal thermogravimetric analysis (TGA) at various heating rates. An approach using a combined kinetics parallel reaction model and model-free isoconversional methods proved to be suitable to determine the pyrolysis kinetic parameters of biomasses with different macromolecular composition and H/C and O/C ratios near 1.5 and 0.8, respectively. Fraser-Suzuki functions representing the derivative TGA (DTG) of hemicellulose, cellulose and lignin showed a very good agreement with the experimental data. The calculated apparent activation energy of biomass pseudo-components evidenced no dependence on the reaction extent in all the conversion range, validating the use of master plots for decomposition mechanism identification. Pseudo-hemicellulose, pseudo-cellulose, and pseudo-lignin showed to be close to a second-order kinetic model, a random scission, or an Avrami-Erofeev model and a high-order kinetic model, respectively. Comparing the three feedstocks, the apparent activation energy of the pseudo-components was in the order: bamboo guadua E_a < coconut shells E_a < oil palm shells E_a . The results show that even when sample elemental composition is very similar, macromolecular constituents, in particular lignin, could have an impact in the biomass decomposition rate and apparent activation energy. For the three studied materials, the model fitting error below 10% showed that the

calculated kinetic parameters are suitable for the description and prediction of the biomass thermal decomposition.

Keywords Kinetic modeling · Parallel reaction model · Pyrolysis · Lignocellulosic biomass · Thermogravimetric analysis

Nomenclature

α	Degree of conversion or reaction extent (–)
A	Frequency factor or pre-exponential factor (min^{-1})
β	Experiment heating rate ($^{\circ}\text{C}/\text{min}$)
BG	Bamboo guadua
c_i	Fraction of each i biomass pseudo-component
CS	Coconut shells
$d\alpha/dt$	Decomposition rate (–)
d_{af}	Dry ash free
E_a	Activation energy (kJ/mol)
OPS	Oil palm shells
R	Ideal gas constant 8.3144 J/mol K
t	Time (min)
T	Temperature ($^{\circ}\text{C}$, K)

Introduction

Thanks to their climate variety, tropical regions have a great biodiversity and the appropriate conditions for the development of agroindustrial activities. Agroindustry produces large amounts of low-cost residues, which can be used for biofuel production or transformed in value-added products. However, in most tropical developing countries, these residues are not valorized and represent an environmental risk, as they are not always disposed properly. According to different studies, the agro-residues potential in developing countries is higher than

✉ Lina María Romero Millán
lromerom@unal.edu.co; lina.romero_millan@mines-albi.fr

¹ Facultad de Ingeniería, Ciudad Universitaria, Universidad Nacional de Colombia–Sede Bogotá, Bogotá, Colombia

² Université de Toulouse, Mines Albi, CNRS, Centre RAPSODEE, Campus Jarlard, Route de Teillet, 81013 Albi Cedex 09, France

2900 million t per year [1]. In Colombia, according to the Colombian Energy and Mining Planning Unit, UPME, more than 70 million t of wastes is produced every year from agroindustrial activities [2]. In this context, the valorization of these residues from an energetic point of view or for the production of value-added products represents an alternative for their treatment and disposal and for strengthening the local economy.

Three Colombian lignocellulosic biomasses were chosen for this study: oil palm shells (OPS), coconut shells (CS), and bamboo guadua (BG). OPS are the shell fractions left after the crushing of the kernel nut in the oil palm extraction process from the *Elaeis guineensis* palm. This biomass is considered an important waste of the Colombian oil palm extraction industry, with near 220,000 t generated every year [2]. In the country, raw OPS are usually burnt in boilers for steam production in palm oil facilities, or disposed as a cover for palm plantation roads, without giving any value to this residue [3]. Furthermore, CS from *Cocos nucifera* palm are considered a material with little or non-economic value from the Colombian alimentary industry, and have been traditionally used for handicraft making or discharged in soils. The amount of this residue is not negligible in the country, considering that near 119,000 t of this fruit is produced in Colombia every year, according to the statistics from the Food and Agriculture Organization of the United Nations [4]. Finally, BG, *Guadua angustifolia* Kunth, is a native woody bamboo species from South and Central America [5, 6]. It has been traditionally used in Colombia as a construction material or firewood. With a high growing rate, BG could represent an interesting material for energy purposes in Colombia and other tropical countries, either from crops or as a residue from the construction industry. Energetic applications of this biomass have not been studied in detail. Reported studies related to bamboo as energy source have been mainly performed with other bamboo species [7–9]. Considering that the three selected biomasses have a heating value above 18 MJ/kg and a great availability [5, 10, 11], it could be interesting to explore their potential to be used as a source of energy, or as a feedstock for the production of value-added materials in Colombia and other tropical countries.

Pyrolysis is the first step in the conversion of biomass into biofuels, adsorbent materials, and value-added chemicals [12–15]. This thermochemical conversion process constitutes the previous stage of combustion and gasification, and should be properly understood for the valorization of different materials through thermochemical conversion processes. In particular, the knowledge of the pyrolysis kinetic parameters is very important to analyze the thermal decomposition process of residual biomasses, predict their conversion, and determine their possible valorization pathways.

Thermogravimetric analysis (TGA) has been widely used for the study of lignocellulosic biomass decomposition

kinetics, either from isothermal and non-isothermal approaches. Several pyrolysis kinetic studies using non-isothermal data have focused on model-free methods to estimate the biomass kinetic parameters, as they allow the evaluation of the activation energy without knowing the decomposition reaction model [16, 17]. However, considering that the biomass pyrolysis is an extremely complex process due to the morphologies of its components and their interaction, the model-free procedure is not always sufficient for the identification of the complete kinetic triplet [18]. Most biomass pyrolysis analysis has reported different activation energy values for several kinds of lignocellulosic biomasses, usually considering only a global decomposition approach [19–22]. Works based on model-free isoconversional methods, showed that there is a clear dependence of activation energy on the reaction extent, suggesting that the pyrolysis process includes many different reactions occurring at the same time. Under these circumstances, an interesting alternative for the analysis of complex conversions is a parallel reaction approach, separating the individual processes by derivative TGA (DTG) peak deconvolution [23], followed by the kinetic analysis of the resulting individual curves. Few studies have been reported for biomass pyrolysis kinetic analysis using DTG deconvolution [24–26]. In particular, BG, CS, and OPS kinetic analysis using this alternative approach has not been reported yet.

According to this, the aim of this work is to study the pyrolysis characteristics and kinetics of three tropical lignocellulosic biomasses, from a non-isothermal TGA. A three-parallel reaction model was employed, using a DTG peak deconvolution procedure, followed by a model-free isoconversional approach and generalized master plots. The influence of the biomass nature in its thermal decomposition characteristics was discussed, comparing the calculated kinetic parameters of the selected materials.

Materials and Methods

Materials

Tropical feedstocks used in this study were collected in Colombia, South America. OPS were provided by a palm oil extraction plant in the Meta region (4° 16' 00" N 73° 29' 00" O, 500 m above sea level, average temperature 27 °C and 2858 mm of precipitation throughout the year). CS from coconuts coming from the Nariño region (1° 10' 00" N 77° 16' 00" O, 0 to 400 m above the sea level and 28 °C of average temperature) were provided by a food processing industry. Both OPS and CS are considered as an industrial residue. For its part, 3- to 4-years-old BG coming from a bamboo forest in the Quindío region (4° 32' 00" N 75° 42' 00" O, 800 to 1200 m above sea level and 23 °C of average

temperature) was obtained from a furniture and handicraft construction site, where biomass was indoor stored.

Raw materials were milled and sieved to a size range of 1 to 2 mm before TGA. CHNS composition of samples was determined using a Thermoquest NA 2000 elemental analyzer. Moisture, volatiles, and ash content were calculated according to the standards EN ISO 18134-3, EN ISO 18123, and EN ISO 18122, respectively. The high heating value was calculated using an IKA C 5000 automated bomb calorimeter. The sample chemical composition and heating value are presented in Table 1 as an average of three replicates. Molecular composition of the biomasses is referred to literature reported values [27–29].

Thermogravimetric Analysis

Thermogravimetric analysis (TGA) of selected materials was performed using a Mettler Toledo TGA 2 SF analyzer. Approximately 30 mg of each sample was placed in an alumina crucible and heated from 25 to 800 °C, with 2, 5, 10, and 20 °C/min as heating rates. Experiments were conducted under a nitrogen atmosphere, using a flow rate of 50 ml/min. To verify the repeatability of TGA experiments, each run was conducted two times and averaged; then, the mean standard deviation was calculated. A blank experiment was made for each heating rate to exclude buoyancy effects. Experimental runs were first performed at 2 °C/min, followed by 5, 10, and 20 °C/min. Duplicates were done following the same order described. For each experimental condition, the standard deviation was below 0.6% for the investigated temperature range. This value was considered reasonable to ensure the repeatability of the obtained mass loss curves.

Kinetic Study

Theoretical Background

TGA has been extensively used to study the kinetics of biomass pyrolysis and to determine the reaction mechanisms controlling this process. Generally, the basis of a kinetic study is a series of experiments where the degree of conversion of a material is measured as a function of time and temperature. According to this, the degree of conversion or reaction extent is usually defined as in Eq. (1).

$$\alpha = \frac{m_0 - m}{m_0 - m_f} \quad (1)$$

where m_0 is the initial mass of the sample, m_f the final mass, and m the current mass at a given temperature or time. The reaction rate $d\alpha/dt$ depends on the temperature T and the degree of conversion α , as shown in Eq. (2). In this expression, $f(\alpha)$ is the reaction model function representing how the solid-

state decomposition process occurs, and $k(T)$ the Arrhenius equation, representing the temperature dependence of the process.

$$\frac{d\alpha}{dt} = k(T)f(\alpha) \quad (2)$$

$$k(T) = A \exp\left(\frac{-E_a}{RT}\right) \quad (3)$$

From the Arrhenius equation (Eq. (3)), the reaction rate expression can be rearranged as follows:

$$\frac{d\alpha}{dt} = A \exp\left(\frac{-E_a}{RT}\right)f(\alpha) \quad (4)$$

Finally, for linear non-isothermal TGA, the reaction rate is expressed as in Eq. 5, where β is the heating rate used to perform the experiment in Kelvin per min.

$$\frac{d\alpha}{dT} = \frac{A}{\beta} \exp\left(\frac{-E_a}{RT}\right)f(\alpha) \quad (5)$$

In the case of biomass decomposition, the most commonly accepted reaction model functions $f(\alpha)$ and their integral forms are presented in Table 2.

Three-Parallel Reaction Model

Thermal decomposition of lignocellulosic biomass is quite complex, considering that it is constituted by different components, mainly hemicellulose, cellulose, and lignin. Accordingly, pyrolysis can be described with a parallel reaction model (PRM), assuming that the three main components of the biomass react independently [31]. Three pseudo-components representing the hemicellulose, cellulose and lignin are then considered in this approach. The total reaction rate is expressed as the addition of each pseudo-component reaction rate, as in Eq. 6.

$$\frac{d\alpha}{dT} = \sum_{i=1}^3 c_i \frac{d\alpha_i}{dT} \quad (6)$$

It is important to note that modeled pseudo-components do not represent the real proportion of biomass constituents, as interactions between them can exist [32]. However, the pseudo-component proportion should be in accordance with each biomass molecular composition.

In order to model these three parallel reactions, the biomass DTG curves were deconvoluted, representing each pseudo-component reaction rate as a mathematical function of temperature. Global DTG curves were then considered as the addition or overlap of pseudo-component DTG profile. Gaussian, Lorentzian, and Fraser-Suzuki functions were used in this study.

Table 1 Heating value and chemical composition of studied biomasses

		OPS	CS	BG
Elemental analysis (wt% daf)	C	46.7 ± 0.2	46.8 ± 0.2	42.7 ± 0.3
	H	6.5 ± 0.1	5.8 ± 0.1	5.4 ± 0.1
	O ^a	46.2 ± 0.1	47.1 ± 0.1	51.5 ± 0.1
	N	0.6 ± 0.1	0.3 ± 0.1	0.4 ± 0.1
	O/C	0.7 ± 0.1	0.7 ± 0.1	0.9 ± 0.1
	H/C	1.7 ± 0.1	1.5 ± 0.1	1.5 ± 0.1
	Proximate analysis (wt%)	Moisture	9.5 ± 0.4	10.2 ± 0.2
Volatile matter		69.9 ± 0.3	71.4 ± 0.3	68.3 ± 0.2
Fixed carbon ^a		19.0 ± 0.3	17.1 ± 0.2	18.1 ± 0.3
Ash		1.6 ± 0.2	1.3 ± 0.1	4.6 ± 0.4
High heating value (MJ/kg)	HHV	19.6 ± 0.2	18.7 ± 0.3	18.0 ± 0.3
Molecular composition (wt% daf)	Cellulose	30.4	32.5	53.9
	Hemicellulose	12.7	20.5	13.5
	Lignin	49.8	36.5	25.1

^a Calculated by difference

Gaussian function [26]:

$$\left(\frac{d\alpha}{dT}\right)_i = a \exp\left[-\frac{1}{2}\left(\frac{T-b}{c}\right)^2\right] \quad (7)$$

where a is the amplitude in 1/K, b is the peak temperature in K, and c is the width of the curve in K.

Lorentzian function [26]:

$$\left(\frac{d\alpha}{dT}\right)_i = \frac{a}{1 + \left(\frac{T-b}{c}\right)^2} \quad (8)$$

where a is the amplitude in 1/K, b is the peak temperature in K, and c is the width of the curve in K.

Fraser-Suzuki function [33]:

$$\left(\frac{d\alpha}{dT}\right)_i = a \exp\left\{-\frac{\ln 2}{d^2} \ln\left[1 + 2d\left(\frac{T-b}{c}\right)\right]^2\right\} \quad (9)$$

where a is the amplitude in 1/K, b is the peak temperature in K, c is the half width of the curve in K, and d is the asymmetry of the curve.

Least square method and an optimization algorithm were used to determine the function parameters that best fit each biomass experimental decomposition profile. The fit error was determined with Eq. 10, where $d\alpha/dT$ are the experimental and

Table 2 Most common reaction mechanisms used in solid-state kinetic analysis related to biomass thermal decomposition

Model		$f(\alpha)$	$g(\alpha)$
Order based	Or1, first order	$1 - \alpha$	$-\ln(1 - \alpha)$
	Or2, second order	$(1 - \alpha)^2$	$[1/(1 - \alpha)] - 1$
	Or3, third order	$(1 - \alpha)^3$	$[1/(1 - \alpha)^2] - 1$
Diffusion	D1, one dimensional	$1/(2\alpha)$	α^2
	D2, two dimensional	$[-\ln(1 - \alpha)]^{-1}$	$\alpha + (1 - \alpha)\ln(1 - \alpha)$
	D3, three dimensional	$(3/2)(1 - \alpha)^{2/3}[1 - (1 - \alpha)^{1/3}]^{-1}$	$[1 - (1 - \alpha)^{1/3}]^2$
	D5, three dimensional	$(3/2)(1 - \alpha)^{4/3}[(1 - \alpha)^{-1/3} - 1]^{-1}$	$[(1 - \alpha)^{-1/3} - 1]^2$
Power law	Pn, power law	$\alpha^{1/2}$	$n(\alpha)^{(n-1)/n}$
Nucleation and growth	An, Avrami-Erofeev	$[-\ln(1 - \alpha)]^{1/n}$	$n(1 - \alpha)[- \ln(1 - \alpha)]^{(n-1)/n}$
Geometrical contraction	R2, Contracting area	$2(1 - \alpha)^{1/2}$	$1 - (1 - \alpha)^{1/2}$
	R3, Contracting volume	$3(1 - \alpha)^{2/3}$	$1 - (1 - \alpha)^{1/3}$
Random scission	L2, Random scission $L = 2$	$2(\alpha^{1/2} - \alpha)$	–

Source: [18, 30]

calculated values of the decomposition rate, and N is the total number of experimental points [32]. According to this, the smaller the fit error, the better fit to the experimental data.

$$Fit\ error\ (\%) = 100 \left(\frac{\sqrt{\sum_{i=1}^N \left(\left(\frac{d\alpha_i}{dT} \right)_{exp} - \left(\frac{d\alpha_i}{dT} \right)_{calc} \right)^2}}{(\sqrt{N}) \left(\frac{d\alpha_i}{dT} \right)_{exp,max}} \right) \quad (10)$$

Once the best fit was determined, isoconversional model-free methods were used for kinetic analysis, as presented in “[Isoconversional Model-Free Approach](#)” section.

Isoconversional Model-Free Approach

In this study, different isoconversional model-free methods were used to determine the Arrhenius parameters from experiments performed with four different heating rates. In particular, three isoconversional methods were compared: Friedman, Flynn-Wall-Ozawa (FWO), and Kissinger-Akahira-Sunose (KAS). Friedman is defined as a differential method, while FWO and KAS are integral methods [18, 34]. All of them are well known and widely used for thermal decomposition kinetic analysis. The activation energy value at a constant α can be calculated from the slope of the isoconversional Arrhenius plots, according to the expressions summarized in Table 3.

If the apparent value of E_a does not vary in a significant way with α , the process can be described by a single-step kinetics, and then, generalized master plots can be used to determine the most suitable reaction mechanism associated and, as a result, the pre-exponential factor A . The reduced-generalized reaction rate expression in Eq. 11 needs the previous knowledge of activation energy value [35].

$$\lambda(\alpha) = \frac{f(\alpha)}{f(\alpha)_{\alpha=0.5}} = \frac{d\alpha/dt}{(d\alpha/dt)_{0.5}} \frac{\exp(E_a/RT)}{\exp(E_a/RT_{0.5})} \quad (11)$$

The most suitable $f(\alpha)$ model can be identified as the best match between the experimental $\lambda(\alpha)$ values and the theoretical master plots presented in Fig. 1 [36].

Results and Discussion

Biomass Composition and Thermal Decomposition Characteristics

In reference to the biomass chemical composition presented in Table 1, it is possible to observe that the three selected materials have similar C and H contents, with H/C ratio between 1.5 and 1.7. In contrast, the molecular composition has remarkable differences, particularly related to lignin content. OPS and CS are endocarp biomasses with relatively high

lignin content (50 and 36%, respectively). In contrast, BG has lignin content below 25% and a high proportion of cellulose (>50%).

Regarding the thermal decomposition behavior, the TG and DTG curves of biomasses are presented in Fig. 2. For the three samples, it is possible to distinguish four decomposition stages. The first one (stage I), registered before 200 °C, is related to the moisture and light volatile release. The second and the third one (stage II and stage III), from 200 to 330 °C and from 300 to 380 °C, correspond mainly to the hemicellulose and cellulose decomposition, and the last one (stage IV), from 380 °C, is mainly related to lignin decomposition. These decomposition ranges found are in accordance with reported values for cellulose, hemicellulose, lignin, and other lignocellulosic biomasses [12, 37].

It is possible to notice from the TG curves that the mass loss in each stage is in agreement with the fraction of hemicellulose, cellulose, and lignin of the samples. In a dry basis, the three biomasses, with similar hemicellulose content, showed a similar mass loss during the second decomposition stage. This value, higher than their reported hemicellulose composition, was expected, taking into account that during this stage, some light volatiles can also be released. Regarding the third stage, BG showed the greatest mass loss, in accordance with its high cellulose content (53.9%). In the same way, the comparison of the TG curves, presented in Fig. 2d, showed that the char yield at the end of the test was different for each biomass. OPS solid residue was 33%, while CS and BG solid yield was 28 and 19%, respectively. These differences could be related to the molecular composition of the samples. It is known that lignin contributes in an important way to the solid yield in biomass decomposition [12], explaining the fact that OPS, with the highest lignin content, registered the lowest mass loss, followed by CS and BG.

Moreover, significant differences can be observed between the DTG curves. In the case of OPS and CS, two distinct peaks can be identified for hemicellulose and cellulose decomposition; while for BG, the hemicellulose decomposition is represented by a shoulder next to the cellulose peak. It should also be noted that as lignin decomposition range occurs over a wide temperature range from 150 to 800 °C [38], no specific lignin peak could be distinguished. Regarding the cellulose decomposition rate, endocarp biomasses showed lower values compared with BG. Taking into account that lignin is the binding agent of biomass fibers, higher lignin contents could be related to lower cellulose decomposition rates and with the well-differentiated decomposition peaks for hemicellulose and cellulose. In relation to this, Lui et al. [39], studied the interaction between biomass components during pyrolysis. They concluded that lignin has a strong effect in hemicellulose and cellulose decomposition. Mendu et al. [40] also found that high lignin biomasses show well-differentiated peaks for hemicellulose and cellulose decomposition.

Table 3 Kinetic model-free methods used in this study

Method	Expression	Isoconversional Arrhenius plot
Friedman	$\ln(d\alpha/dt) = \ln[A f(\alpha)] - E_a/RT$	$\ln(\beta d\alpha/dT)$ Vs $1/T$
Kissinger-Akahira-Sunose (KAS)	$\ln(\beta/T^2) = \ln(A R/E_a g(\alpha)) - E_a/RT$	$\ln(\beta/T^2)$ Vs $1/T$
Flynn-Wall-Ozawa (FWO)	$\log\beta = \log(A E_a/R g(\alpha)) - 2.315 - 0.4567 E_a/RT$	$\text{Log}\beta$ Vs $1/T$

DTG Curve Deconvolution

Biomass DTG curves were deconvoluted, representing each pseudo-component with Gaussian, Lorentzian, and Fraser Suzuki functions. As Gaussian and Lorentzian functions are symmetric, they were particularly inadequate to fit the OPS and CS decomposition patterns, with an error greater than 13 and 15%, respectively. In contrast, Fraser-Suzuki function allowed the fitting of asymmetric curves, giving a good agreement with experimental data. In all cases, the fit error was lower than 3%. Parejon et al. [23] found that Fraser-Suzuki function is the mathematical algorithm that better fits the decomposition rate patterns of complex processes. Figure 3 presents the results of the Fraser-Suzuki deconvolution fitting of BG, CS, and OPS at a heating rate of 10 °C/min. Table 4 summarizes the final parameters that better fitted each experimental data set.

From the deconvolution results, the pseudo-hemicellulose, pseudo-cellulose, and pseudo-lignin fractions of biomass samples were calculated. BG values were 32, 49, and 19%, respectively. CS values were 28, 29, and 42%, and finally, OPS values were 26, 24, and 50%. It should be noted that even when modeled pseudo-components do not represent the real proportion of biomass constituents, their fractions show the different nature of the studied samples in terms of their molecular composition.

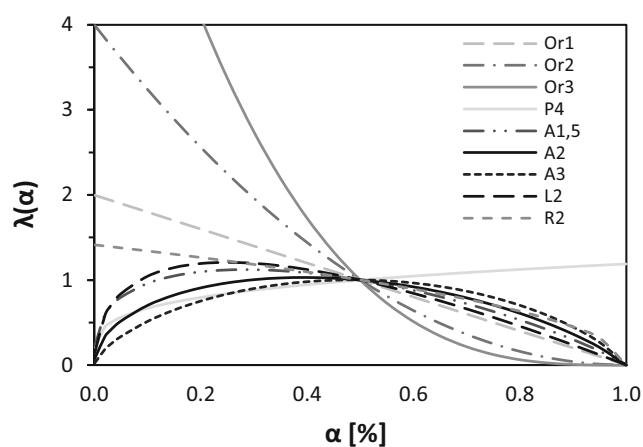


Fig. 1 Generalized master plots of the different kinetic models in Table 2, constructed according to Eq. 6

Kinetic Analysis

For the selected biomasses, decomposition rate curves ($d\alpha/dT$ Vs T) of each pseudo-component were analyzed using isoconversional model-free methods, in order to determine their kinetic triplet E_a , A , and $f(\alpha)$. Friedman, KAS, and FWO Arrhenius plots for OPS, CS, and BG pseudo-components showed a good linear fit in all the conversion range between 0.1 and 0.9. In all cases, R^2 values were higher than 0.9871, as presented in Table 5, where the maximum and minimum R^2 values are summarized. The high correlation coefficients R^2 obtained suggest that the three isoconversional methods used are reliable and accurate for the apparent activation energy calculation.

Biomass pseudo-component E_a was determined from the slope of the isoconversional plot regression lines, according to the Friedman, KAS, and FWO methods, presented in Table 3. The calculated E_a values are shown in Fig. 4, as a function of the reaction extent.

It is possible to observe that in all cases, the dependence of E_a on α is quite low. The apparent activation energy remained almost constant in all the conversion range, indicating that pseudo-component thermal decomposition follows a single-stage process and no complex reactions occur [30]. In relation to this, Table 6 summarizes the mean activation energy value found for the three biomass pseudo-components, using the described isoconversional methods. It should be noted that the relative standard deviation of the activation energy was always lower than 8% ($\sigma = 13.5$ kJ/mol), with values even below 2% ($\sigma = 3.2$ kJ/mol).

Friedman, KAS, and FWO approaches gave similar apparent activation energy values with absolute deviation below 11% in all cases. These results show that all the three methods are convenient for the calculation of the activation energy of the sample pseudo-component decomposition. In particular, it can be said that for biomasses with H/C and O/C near 1.6 and 0.8, any of the presented methods is suitable for the determination of pyrolysis kinetic parameters, despite the differences in hemicellulose, cellulose, and lignin fractions and their decomposition behavior.

The highest absolute deviation between the methods was found for the mean E_a calculated with Friedman and FWO for OPS pseudo-hemicellulose (22.4 kJ/mol—10.5%). In contrast, the results obtained with KAS and FWO were very close, with deviations below 1%. These differences are related

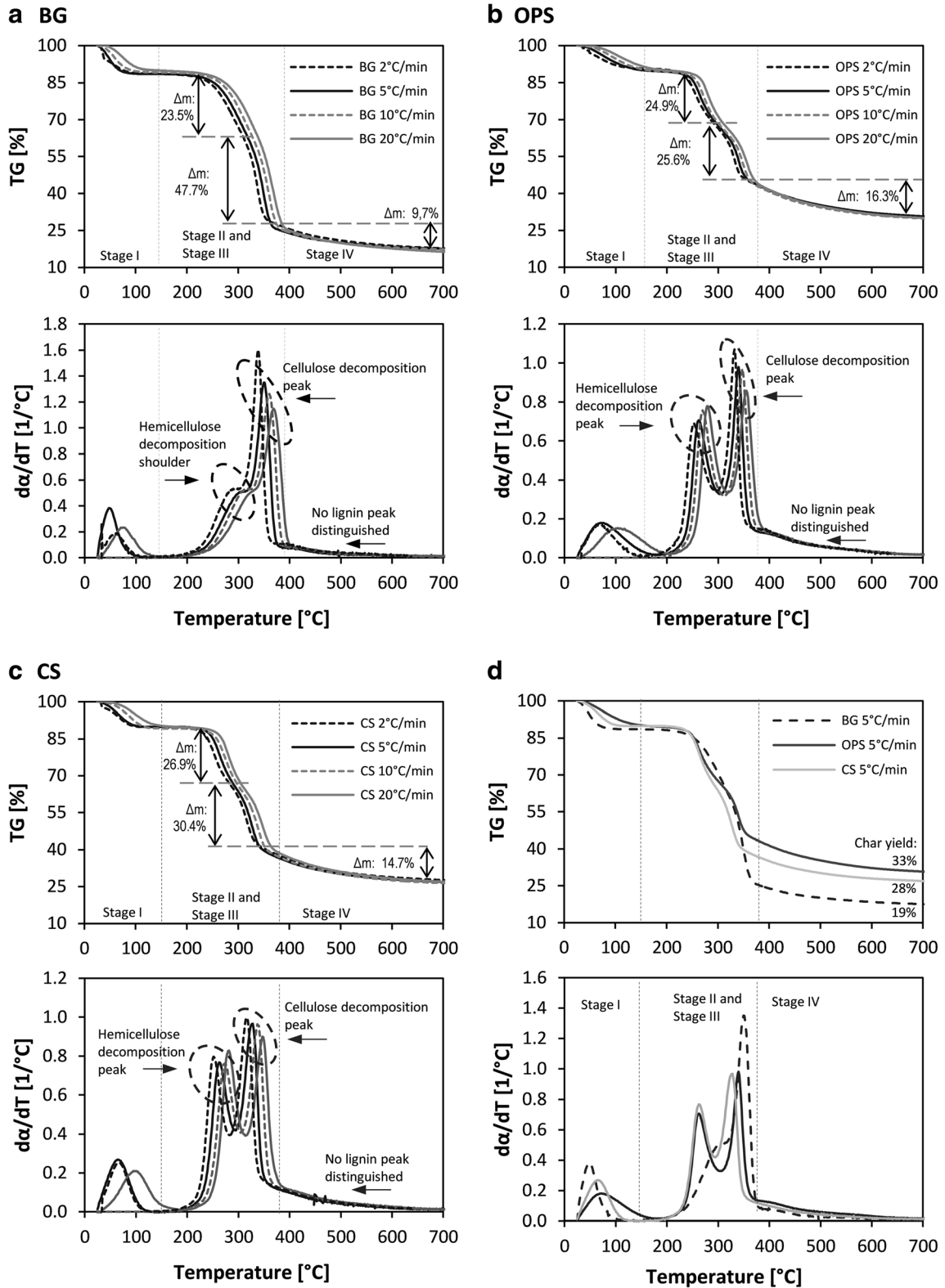


Fig. 2 TG and DTG curves at 2, 5, 10, and 20 °C/min. **a** *Guadua angustifolia* Bamboo guadua (BG). **b** Oil palm shells (OPS). **c** Coconut shells (CS). **d** Comparison of TG and DTG curves at 5 °C/min. Mass loss values and char yield are presented in a dry basis

to the mathematical approach of the isoconversional methods and the treatment of the experimental data, considering that

Friedman is a differential method while FWO and KAS are integral.

Table 4 Fitting results of Fraser-Suzuki deconvolution of selected biomasses

	Parameters	BG			CS			OPS		
		P-HC	P-C	P-L	P-HC	P-C	P-L	P-HC	P-C	P-L
2 °C/min	a (1/K)	-0.450	-1.460	-0.110	-0.620	-0.795	-0.169	-0.520	-0.840	-0.220
	b (°K)	283.0	337.7	359.0	251.0	315.0	293.0	251.5	328.5	301.0
	c (°K)	57.0	23.0	180.0	36.5	26.0	175.0	35.8	20.5	182.0
	d (-)	-0.200	-0.420	0.210	0.350	-0.300	0.555	0.360	-0.400	0.630
	Fit error (%)	1.8			2.0			2.1		
5 °C/min	a (1/K)	-0.428	-1.266	-0.073	-0.620	-0.795	-0.165	-0.550	-0.788	-0.184
	b (°K)	297.5	350.5	370.5	262.5	327.5	304.0	262.0	339.2	309.0
	c (°K)	56.0	25.5	186.0	37.0	26.0	180.0	34.7	22.0	184.0
	d (-)	-0.200	-0.400	0.200	0.350	-0.300	0.555	0.390	-0.345	0.630
	Fit error (%)	1.6			1.2			1.5		
10 °C/min	a (1/K)	-0.440	-1.180	-0.075	-0.620	-0.797	-0.165	-0.600	-0.776	-0.185
	b (°K)	308.5	360.8	380.5	272.5	338.0	312.5	269.8	347.1	319.5
	c (°K)	56.0	26.5	190.0	37.0	26.0	185.0	33.5	21.0	190.0
	d (-)	-0.200	-0.400	0.200	0.330	-0.300	0.560	0.420	-0.295	0.620
	Fit error (%)	1.9			1.0			1.8		
20 °C/min	a (1/K)	-0.420	-1.040	-0.075	-0.660	-0.734	-0.165	-0.630	-0.682	-0.180
	b (°K)	318.8	371.7	391.0	281.5	347.8	319.0	279.5	356.4	325.7
	c (°K)	56.0	29.0	196.0	38.0	26.0	190.0	36.0	24.0	196.0
	d (-)	-0.200	-0.370	0.210	0.350	-0.300	0.570	0.360	-0.280	0.630
	Fit error (%)	2.0			1.7			2.1		

P-HC pseudo-hemicellulose, *P-C* pseudo-cellulose, *P-L* pseudo-lignin

From Table 6, it is also possible to notice that for the three biomasses, pseudo-component decomposition followed nearly the same behavior, as E_a is in the order: E_a pseudo-hemicellulose < E_a pseudo-cellulose < E_a pseudo-lignin. Keeping in mind that E_a is the minimum energy required to start a reaction, the lower pseudo-hemicellulose E_a value means that this component degrades easier than the two others. Accordingly, it is possible to see from Fig. 4 that pseudo-hemicellulose decomposition starts at a lower temperature than that of pseudo-cellulose and pseudo-lignin. For its part, pseudo-lignin decomposition over a large temperature range indicates that this component degrades slowly, and is

harder to decompose than pseudo-hemicellulose and pseudo-cellulose. The high E_a values associated with pseudo-lignin could be related to its aromatic nature and the fact that this component is the cementing agent of biomass fibers. Lignin is a complex three-dimensional polymer with a large variety of chemical functions which differ in thermal stability and decompose in a broad temperature range [41], interacting with cellulose and hemicellulose. These interactions during biomass decomposition may explain the fact that calculated pseudo-lignin activation energy is higher than isolated lignin reported values, which can be in the range of 37 to 160 kJ/mol, depending on the analyzed lignin type [42, 43].

Table 5 R^2 correlation coefficient of isoconversional Arrhenius plots for the three studied biomasses

		Pseudo-hemicellulose			Pseudo-cellulose			Pseudo-lignin		
		Friedman	KAS	FWO	Friedman	KAS	FWO	Friedman	KAS	FWO
BG	R^2 min	0.9977	0.9982	0.9982	0.9942	0.9986	0.9988	0.9906	0.9871	0.9981
	R^2 max	0.9997	1.0000	1.0000	1.0000	1.0000	1.0000	0.9976	0.9992	0.9993
CS	R^2 min	0.9971	0.9990	0.9984	0.9977	0.9989	0.9989	0.9950	0.9946	0.9950
	R^2 max	0.9997	1.0000	1.0000	0.9996	0.9997	0.9998	0.9991	0.9994	0.9995
OPS	R^2 min	0.9973	0.9983	0.9984	0.9940	0.9977	0.9971	0.9903	0.9918	0.9938
	R^2 max	1.0000	1.0000	1.0000	0.9991	0.9997	1.0000	0.9999	0.9999	0.9999

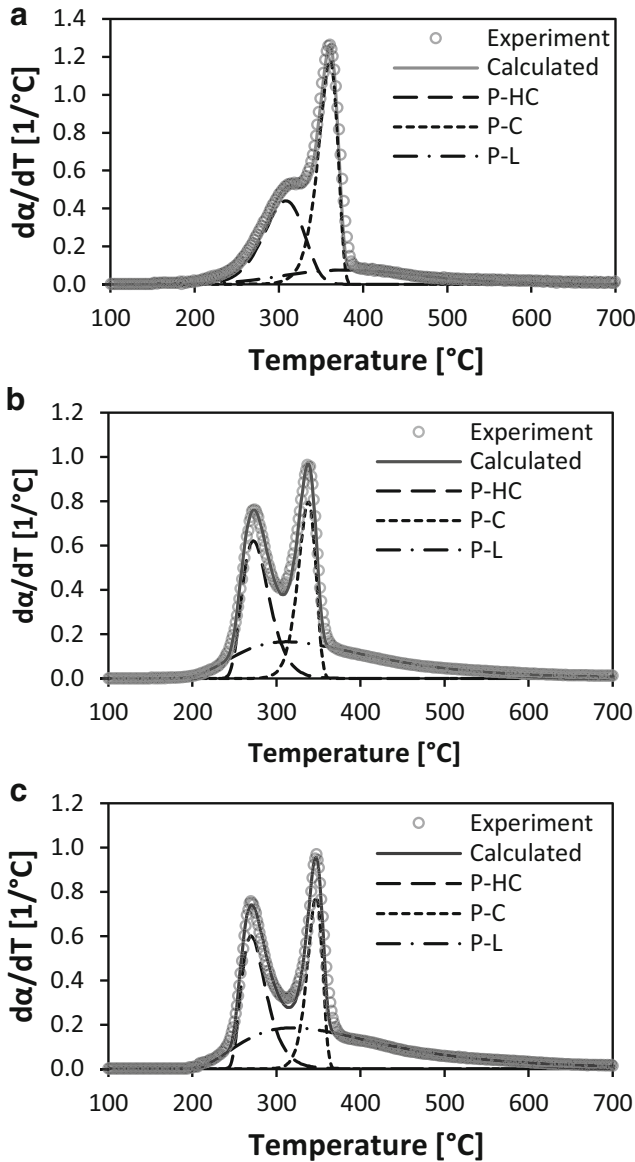


Fig. 3 Comparison between experimental curves and Fraser-Suzuki deconvolution results of **a** BG at 10 °C/min, **b** CS at 10 °C/min, and **c** OPS at 10 °C/min. *P-HC* pseudo-hemicellulose, *P-C* pseudo-cellulose, *P-L* pseudo-lignin

The apparent activation energies obtained with the three employed methods were in accordance with different biomass pseudo-component values in the literature. Reported pseudo-hemicellulose activation energy is between 86 and 180 kJ/mol, pseudo-cellulose between 140 and 210 kJ/mol, and pseudo-lignin between 62 and 230 kJ/mol [24, 44–47]. However, it can be observed that there are some differences between the three studied biomass samples. In particular, OPS is the material that presented the highest activation energy for the three pseudo-components, followed by CS and then by BG. OPS pseudo-hemicellulose E_a is near 15 and 20% higher than CS and BG in that order. OPS pseudo-cellulose value is greater than CS and BG in around 10 and 17% and pseudo-lignin value in around 5 and 10%, respectively.

This behavior could be possibly explained by the interactions between the biomass components and structure, during thermal decomposition. As the binding agent for biomass structure, lignin could have an impact in the required energy to decompose hemicellulose and cellulose. In relation to this, OPS have the highest lignin content between the studied biomasses and presented the highest E_a values, while BG has the lowest lignin content and the lowest E_a for the three pseudo-components. Thus, it is possible to infer that even when the three studied materials are mainly constituted by the same components, biomass structure plays a role in their decomposition characteristics [48, 49].

According to this, the most suitable decomposition reaction model for each biomass pseudo-component was determined using the generalized master plots procedure, which is valid only for single-stage process analysis, where there is no dependence of E_a on α [18]. Experimental data were normalized to $\alpha = 0.5$ using Eq. 6, and compared with theoretical master plots in Fig. 1. Activation energy in Eq. 6 is the mean value calculated for each pseudo-component using the mentioned three isoconversional methods.

Figure 5a shows that for the three biomasses, pseudo-hemicellulose matches closely the theoretical plot of a second-order kinetic model (Or2), except at low conversion ($\alpha < 0.2$), where the decomposition model of OPS and CS

Table 6 Mean activation energy values of OPS, CS, and BG pseudo-components, calculated using Friedman, KAS, and FWO model-free methods

Apparent activation energy: E_a (kJ/mol), σ (kJ/mol)

	Pseudo-hemicellulose			Pseudo-cellulose			Pseudo-lignin		
	Friedman	KAS	FWO	Friedman	KAS	FWO	Friedman	KAS	FWO
BG	167.8 $\sigma = 1.1$	163.2 $\sigma = 12.2$	164.2 $\sigma = 11.9$	191.0 $\sigma = 7.1$	211.3 $\sigma = 6.2$	210.7 $\sigma = 5.8$	198.4 $\sigma = 5.8$	221.2 $\sigma = 7.0$	221.0 $\sigma = 7.5$
CS	189.9 $\sigma = 10.0$	175.9 $\sigma = 8.2$	175.9 $\sigma = 8.0$	222.5 $\sigma = 6.8$	219.8 $\sigma = 6.5$	218.5 $\sigma = 6.3$	235.8 $\sigma = 4.4$	228.3 $\sigma = 3.9$	226.9 $\sigma = 4.8$
OPS	217.0 $\sigma = 10.5$	195.8 $\sigma = 11.4$	194.6 $\sigma = 10.7$	234.1 $\sigma = 7.8$	240.0 $\sigma = 3.3$	240.9 $\sigma = 3.2$	237.3 $\sigma = 7.6$	249.5 $\sigma = 5.8$	248.2 $\sigma = 6.5$

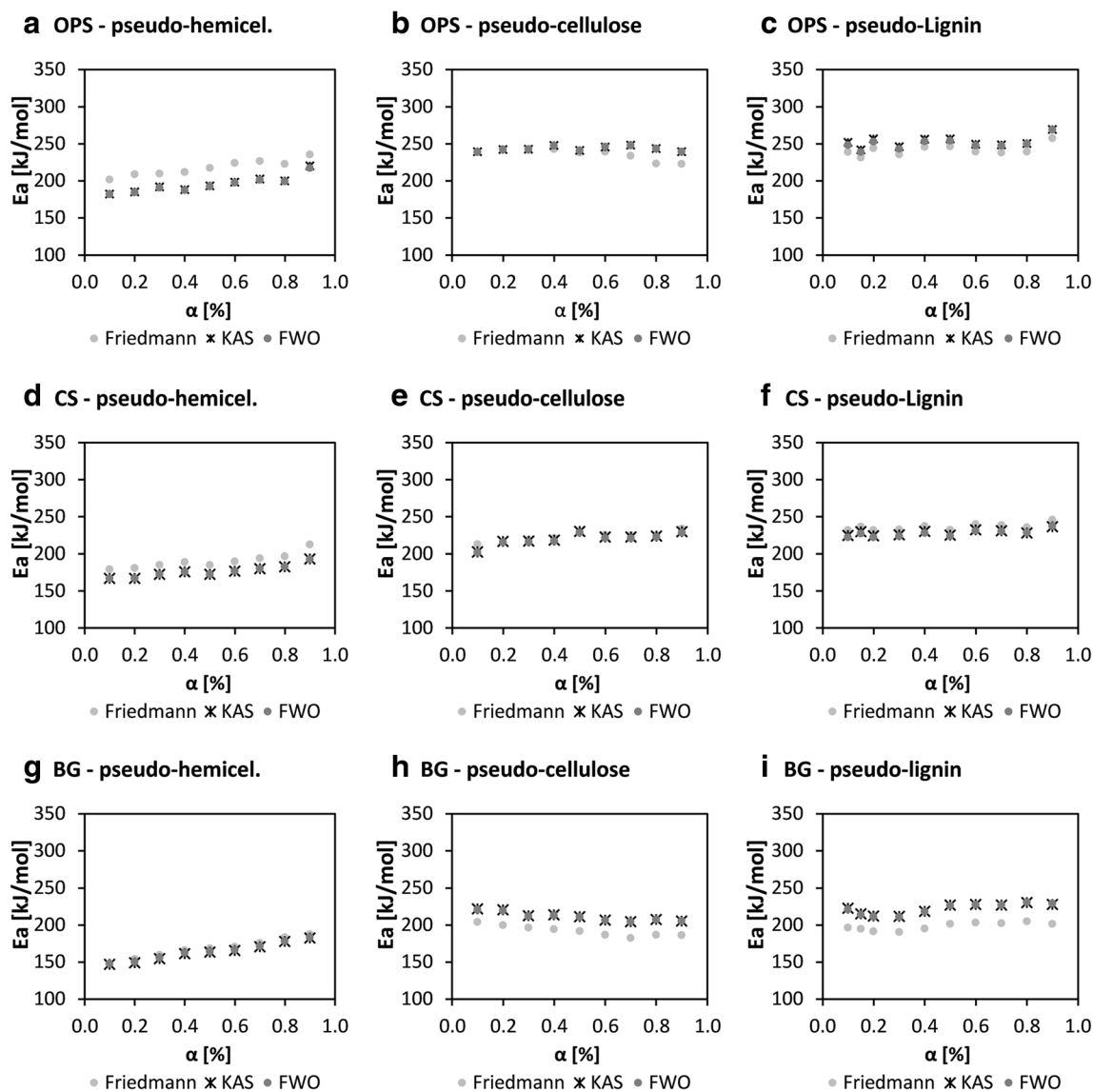


Fig. 4 Apparent activation energy values of BG, CS and OPS pseudo-components, as a function of reaction extent

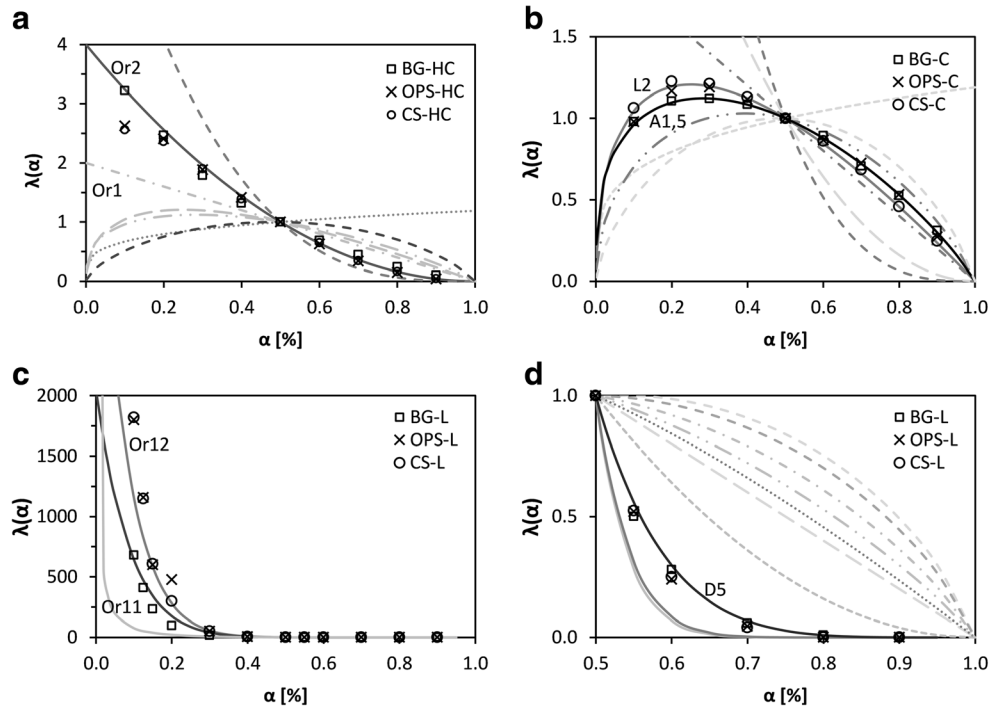
pseudo-hemicellulose is between first order and second order. For its part, BG is close to a second-order kinetic model in all the decomposition range. These differences at low conversion could be possibly due to interactions between the hemicellulose and the other biomass components. Similar approaches to other types of lignocellulosic biomasses have concluded that pseudo-hemicellulose decomposition follows an order-based kinetic model with n between 1.5 and 4 [50].

Master plots in Fig. 5b show that pseudo-cellulose decomposition is in agreement with a random scission or an Avrami-Erofeev kinetic model, for the three studied biomasses. Notably, BG pseudo-cellulose matches better with an A1.5 Avrami-Erofeev nucleation and growth model, while OPS and CS pseudo-cellulose are closer to a L2 random scission model. Theoretical master plots of both models are close and are related to narrow reaction profiles, as seen in Fig. 4, where pseudo-cellulose decomposition range is narrower compared with

pseudo-hemicellulose and pseudo-lignin. In general, Avrami-Erofeev models assume that reaction or decomposition is due to the appearance of random nuclei and their subsequent growth, while random scission is related to the arbitrary break of polymer chains into smaller segments [30, 51]. As the shape of both models is very close, it is not easy to consistently distinguish between them, in spite of the differences in their theoretical background. According to this, from a mathematical point of view, both of these models could describe the pseudo-cellulose decomposition mechanism. Similar studies reported for cellulose in the literature have concluded that both Avrami-Erofeev and random scission models could be suitable for the description of the cellulose thermal decomposition [22, 36, 52].

Finally, as seen in Fig. 5c, pseudo-lignin decomposition does not match with any known theoretical kinetic model. Due to the complexity of the lignin structure and its interactions with the other biomass components [44, 48, 49], it

Fig. 5 Comparison between the experimental and theoretical master plots for the three biomass pseudo-components. **a** Pseudo-hemicellulose. **b** Pseudo-cellulose. **c** Pseudo-lignin. **d** Pseudo-lignin ($0.5 < \alpha < 1.0$)



is not easy to fully understand its decomposition mechanism. As the cementing agent of biomass, lignin could interact with hemicellulose and cellulose in different ways according to the biomass structure and operating conditions. Moreover, lignin decomposes in a wide range of temperature and with low decomposition rate, making it difficult to completely model its corresponding reaction mechanism. At low conversion ($\alpha < 0.5$), pseudo-lignin decomposition could be modeled by an order reaction mechanism, with n between 11 and 12 (Fig. 5c). From $\alpha = 0.5$ to $\alpha = 0.9$, decomposition is near a three-dimensional diffusion mechanism. Particularly, a D5 model (Zhuravlev, Lesokin, Tempelman), as presented in Fig. 5d. Other reported studies have described pseudo-lignin decomposition with a third-order reaction model [24], or even a high-order model with $n > 12$ [22]. The

proposed models, however, do not fit completely the pseudo-lignin the decomposition, due to its complexity.

With the knowledge of the most suitable reaction model for each pseudo-component, pre-exponential factor A values were calculated. Taking into account that the difference between the apparent activation energy calculated with the Friedman, KAS, and FWO methods is not significant, E_a of each biomass pseudo-component was defined as the mean value of the activation energy estimated with the three methods. Furthermore, the Friedman method was chosen for the evaluation of the pre-exponential factor.

The dependence of $\ln(A)$ on α , presented in Fig. 6, is similar to that of the activation energy, remaining almost constant during all the conversion range ($0.1 < \alpha < 0.9$). The relative standard deviation was in all cases inferior to 8% with

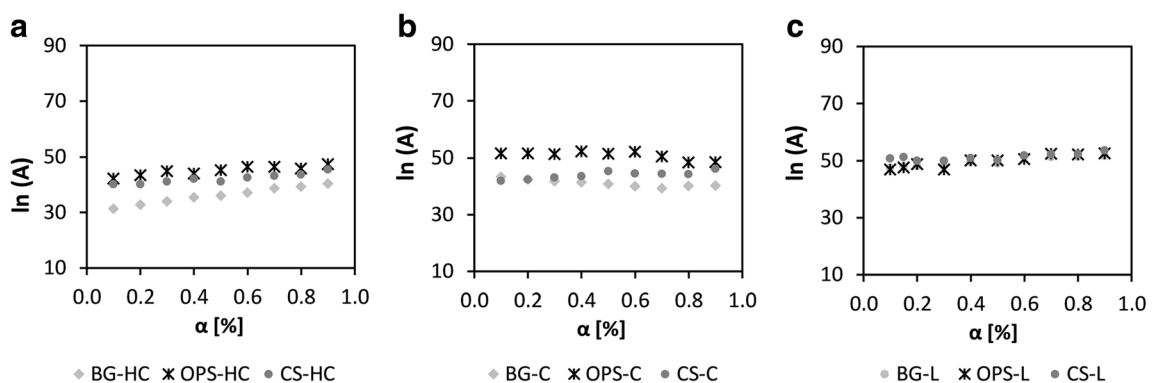


Fig. 6 Pseudo-component dependence of $\ln(A)$ on the reaction extent. **a** Pseudo-hemicellulose. **b** Pseudo-cellulose. **c** Pseudo-lignin

Table 7 Average E_a and A values calculated for BG, CS, and OPS pseudo-components

Biomass	Pseudo-hemicellulose		Pseudo-cellulose		Pseudo-lignin	
	E_a (kJ/mol)	A (s^{-1})	E_a (kJ/mol)	A (s^{-1})	E_a (kJ/mol)	A (s^{-1})
BG	165.1	2.62E+14	204.3	2.30E+16	214.5	1.02E+18
CS	180.6	5.83E+16	220.3	2.30E+18	230.3	1.47E+21
OPS	202.4	6.33E+18	238.1	3.50E+19	245.0	8.83E+21

values of even 2%. Accordingly, the mean values of E_a and A for the three biomasses are summarized in Table 7.

These kinetic parameters were validated and used to reproduce the experimental decomposition curves of each biomass from 2 to 20 °C/min. For the three studied materials, a good agreement was found between the experimental data and the computed decomposition behavior, with fitting errors below 10% in all cases. Figure 7 shows the modeled decomposition rate of the three biomasses and pseudo-components at a heating rate of 10 °C/min.

It is possible to observe from this figure that there is a gap between experimental and modeled data at temperatures

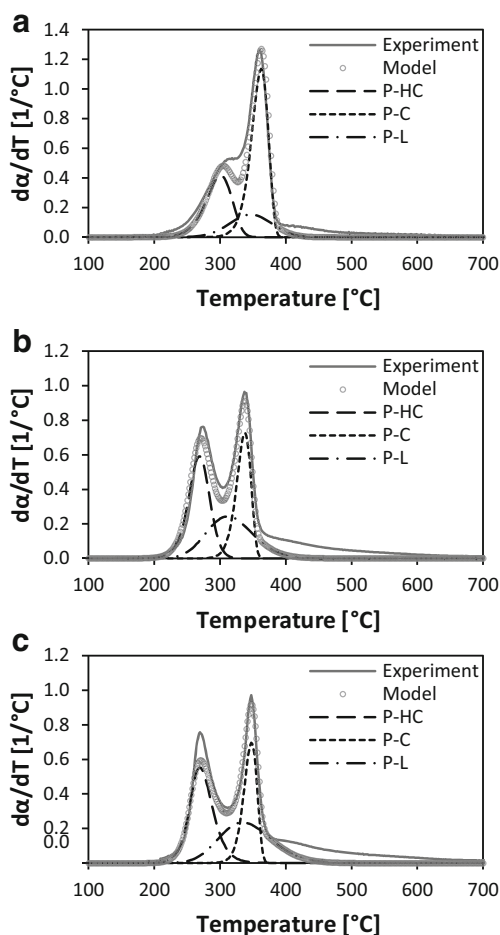


Fig. 7 Comparison between experimental and modeled decomposition curves of **a** BG at 10 °C/min, **b** CS at 10 °C/min, and **c** OPS at 10 °C/min. Modeled curves generated using the calculated E_a and A values presented in Table 7 for biomasses and their pseudo-components

above 400 °C, for the three biomasses. Comparing these results with Fraser-Suzuki fitting presented in Fig. 4, it can be noticed that the behavior of modeled pseudo-hemicellulose and pseudo-cellulose is in good agreement with the deconvolution patterns initially proposed. As a result, a good agreement is also obtained between modeled and experimental decomposition at temperatures below 400 °C. In contrast, it is clear that the main differences observed are related to pseudo-lignin. This is principally due to the complexity of modeling the pseudo-lignin decomposition behavior in the investigated temperature range. In spite of this, the fitting error below 10% for the three materials showed that the calculated kinetic parameters using model-free isoconversional methods are suitable for the description of the biomass thermal decomposition.

Conclusion

In this study, the thermal decomposition of three lignocellulosic biomasses with different macromolecular composition but nearly the same H/C and O/C fraction was investigated. Bamboo guadua (BG), coconut shells (CS), and oil palm shells (OPS) were used.

In general, the approach presented in this paper using a PRM using Fraser-Suzuki deconvolution and model-free isoconversional methods proved to be suitable to determine the pyrolysis kinetic parameters of biomasses with H/C and O/C near 1.5 and 0.8. Despite the differences in the hemicellulose, cellulose, and lignin fraction of biomasses, any of the presented isoconversional methods can be used to calculate and predict the pseudo-component activation energy and pre-exponential factor, and to estimate their decomposition mechanism. This information could constitute a valuable tool for reactor design and for the development and scale-up of pyrolysis and gasification processes using tropical lignocellulosic agrowastes as a feedstock.

The apparent activation energy of biomass pseudo-components followed the same behavior for the three studied materials: pseudo-hemicellulose $E_a <$ pseudo-cellulose $E_a <$ pseudo-lignin E_a . Regarding the decomposition mechanism, pseudo-hemicellulose and pseudo-cellulose were well described by a second-order model and a random-scission or an A1.5 Avrami-Erofeev model, respectively. For its part, pseudo-lignin decomposition did not completely match with

any known theoretical model, and was described by a combination of a high-order model with n between 11 and 12 and a third dimension diffusion model. Lignin behavior was possibly due to the complexity of its structure and to the interactions with the other biomass components.

Differences between the calculated kinetic parameters of BG, CS, and OPS showed that biomass structure and molecular composition play a role in the biomass decomposition characteristics. Considering the nature of lignin, it could have an impact in the required energy to decompose hemicellulose and cellulose. The apparent activation energy for the three biomass pseudo-components followed the order BG $E_a < CS < OPS$, with OPS and BG being the highest lignin and lowest lignin content biomasses analyzed in this study, respectively. For the three studied materials, the model fitting error below 10% showed that the calculated kinetic parameters using model-free isoconversional methods are suitable for the description and prediction of the biomass thermal decomposition.

Acknowledgements The authors gratefully acknowledge COLCIENCIAS, for the doctoral scholarship awarded in the frame of the Colombian National Program for Doctoral Formation 647-2014.

References

- Ullah K, Kumar Sharma V, Dhingra S et al (2015) Assessing the lignocellulosic biomass resources potential in developing countries: a critical review. *Renew Sust Energ Rev* 51:682–698. doi:10.1016/j.rser.2015.06.044
- Escalante H, Orduz J, Zapata HJ, et al (2010) Potencial energético de la biomasa residual. In: Ministerio de Minas y Energía - Republica de Colombia (ed) Atlas del Potencial Energético Biomasa Residual en Colomb. pp 155–172
- García NJ a, EE YA (2010) Generación y uso de biomasa en plantas de beneficio de palma de aceite en Colombia—Power generation and use of biomass at palm oil mills in Colombia. *Rev Palmas* 31: 41–48
- Food and Agriculture Organisation of the United Nations (2014) FAO statistical yearbook 2014: Latin America and the Caribbean. Santiago de Chile
- Fryda L, Daza C, Pels J et al (2014) Lab-scale co-firing of virgin and torrefied bamboo species *Guadua angustifolia* Kunth as a fuel substitute in coal fired power plants. *Biomass Bioenergy* 65:28–41. doi:10.1016/j.biombioe.2014.03.044
- Londoño X, Camayo GC, Riaño N, López Y (2002) Characterization of the anatomy of *Guadua angustifolia* (Poaceae: Bambusoideae) culms. *Bamboo Sci Cult* 16:18–31
- Kuo P-C, Wu W, Chen W-H (2014) Gasification performances of raw and torrefied biomass in a downdraft fixed bed gasifier using thermodynamic analysis. *Fuel* 117:1231–1241. doi:10.1016/j.fuel.2013.07.125
- Wongsiriamnuay T, Kannang N, Tippayawong N (2013) Effect of operating conditions on catalytic gasification of bamboo in a fluidized bed. *Int J Chem Eng*. doi:10.1155/2013/297941
- Chen D, Liu D, Zhang H et al (2015) Bamboo pyrolysis using TG–FTIR and a lab-scale reactor: analysis of pyrolysis behavior, product properties, and carbon and energy yields. *Fuel* 148:79–86. doi:10.1016/j.fuel.2015.01.092
- Forero Núñez CA, Cediell A, Hernández LC, et al (2012) Oil palm empty bunch fruits and coconut shells gasification using a lab-scale downdraft fixed bed gasifier at Universidad Nacional de Colombia. In: 20th Eur. Conf. Exhib. Milan, Italy, pp 1112–1114
- Romero Millán LM, Cruz Domínguez MA, Sierra Vargas FE (2016) Efecto de la temperatura en el potencial de aprovechamiento energético de los productos de la pirólisis del cuesco de palma. *Rev Tecnura* 20:89–99. doi:10.14483/udistrital.jour.tecnura.2016.2.a06
- Basu P (2013) Pyrolysis. In: Biomass gasification, pyrolysis and torrefaction, Second Edi. Elsevier Inc., London, pp 147–176
- David E, Kopac J (2014) Activated carbons derived from residual biomass pyrolysis and their CO₂ adsorption capacity. *J Anal Appl Pyrolysis* 110:322–332. doi:10.1016/j.jaap.2014.09.021
- Ye L, Zhang J, Zhao J et al (2015) Properties of biochar obtained from pyrolysis of bamboo shoot shell. *J Anal Appl Pyrolysis* 114: 172–178. doi:10.1016/j.jaap.2015.05.016
- Abnisa F, Arami-Niya A, Wan Daud WMA et al (2013) Utilization of oil palm tree residues to produce bio-oil and bio-char via pyrolysis. *Energy Convers Manag* 76:1073–1082. doi:10.1016/j.enconman.2013.08.038
- White JE, Catallo WJ, Legendre BL (2011) Biomass pyrolysis kinetics: a comparative critical review with relevant agricultural residue case studies. *J Anal Appl Pyrolysis* 91:1–33. doi:10.1016/j.jaap.2011.01.004
- Vyazovkin S, Wight CA (1999) Model-free and model-fitting approaches to kinetic analysis of isothermal and nonisothermal data. *Thermochim Acta* 340:53–68. doi:10.1016/S0040-6031(99)00253-1
- Vyazovkin S, Burnham AK, Criado JM et al (2011) ICTAC kinetics committee recommendations for performing kinetic computations on thermal analysis data. *Thermochim Acta* 520:1–19. doi:10.1016/j.tca.2011.03.034
- Huang X, Cao J-P, Zhao X-Y et al (2016) Pyrolysis kinetics of soybean straw using thermogravimetric analysis. *Fuel* 169:93–98. doi:10.1016/j.fuel.2015.12.011
- Ma Z, Chen D, Gu J et al (2015) Determination of pyrolysis characteristics and kinetics of palm kernel shell using TGA–FTIR and model-free integral methods. *Energy Convers Manag* 89:251–259. doi:10.1016/j.enconman.2014.09.074
- Słowiecka K, Bartocci P, Fantozzi F (2012) Thermogravimetric analysis and kinetic study of poplar wood pyrolysis. *Appl Energy* 97:491–497. doi:10.1016/j.apenergy.2011.12.056
- Wang X, Hu M, Hu W et al (2016) Thermogravimetric kinetic study of agricultural residue biomass pyrolysis based on combined kinetics. *Bioresour Technol* 219:510–520. doi:10.1016/j.biortech.2016.07.136
- Perejón A, Sánchez-Jiménez PE, Criado JM, Pérez-Maqueda LA (2011) Kinetic analysis of complex solid-state reactions. A new deconvolution procedure. *J Phys Chem B* 115:1780–1791. doi:10.1021/jp110895z
- Hu M, Chen Z, Wang S et al (2016) Thermogravimetric kinetics of lignocellulosic biomass slow pyrolysis using distributed activation energy model, Fraser–Suzuki deconvolution, and iso-conversional method. *Energy Convers Manag* 118:1–11. doi:10.1016/j.enconman.2016.03.058
- Janković B (2015) Devolatilization kinetics of swine manure solid pyrolysis using deconvolution procedure. Determination of the bio-oil/liquid yields and char gasification. *Fuel Process Technol* 138:1–13. doi:10.1016/j.fuproc.2015.04.027
- Taghizadeh MT, Yeganeh N, Rezaei M (2014) Kinetic analysis of the complex process of poly(vinyl alcohol) pyrolysis using a new coupled peak deconvolution method. *J Therm Anal Calorim* 118: 1733–1746. doi:10.1007/s10973-014-4036-4

27. Cuéllar A, Muñoz I (2010) Fibra de guadua como refuerzo de matrices poliméricas - Bamboo fiber reinforcement for polymer matrix. *DYNA* 77:137–142. doi:10.15446/dyna
28. Mortley Q, Mellowes WA, Thomas S (1988) Activated carbons from materials of varying morphological structure. *Thermochim Acta* 129:173–186. doi:10.1016/0040-6031(88)87334-9
29. García-Núñez JA, García-Pérez M, Das KC (2008) Determination of kinetic parameters of thermal degradation of palm oil mill by-products using thermogravimetric analysis and differential scanning calorimetry. *Trans ASABE* 51:547–557. doi:10.13031/2013.24354
30. Brown ME (1998) Handbook of thermal analysis and calorimetry. Volume 1. Principles and practice, First Edit. Elsevier
31. Anca-Couce A, Berger A, Zobel N (2014) How to determine consistent biomass pyrolysis kinetics in a parallel reaction scheme. *Fuel* 123:230–240. doi:10.1016/j.fuel.2014.01.014
32. Anca-Couce A, Zobel N, Berger A, Behrendt F (2012) Smouldering of pine wood: kinetics and reaction heats. *Combust Flame* 159:1708–1719. doi:10.1016/j.combustflame.2011.11.015
33. Svoboda R, Málek J (2013) Applicability of Fraser–Suzuki function in kinetic analysis of complex crystallization processes. *J Therm Anal Calorim* 111:1045–1056. doi:10.1007/s10973-012-2445-9
34. Rajeshwari P, Dey TK (2016) Advanced isoconversional and master plot analyses on non-isothermal degradation kinetics of AlN (nano)-reinforced HDPE composites. *J Therm Anal Calorim* 125:369–386. doi:10.1007/s10973-016-5406-x
35. Gotor FJ, Criado JM, Malek J, Koga N (2000) Kinetic analysis of solid-state reactions: the universality of master plots for analyzing isothermal and nonisothermal experiments. *J Phys Chem A*:10777–10782. doi:10.1021/jp0022205
36. Sánchez-Jiménez PE, Pérez-Maqueda LA, Perejón A, Criado JM (2013) Generalized master plots as a straightforward approach for determining the kinetic model: the case of cellulose pyrolysis. *Thermochim Acta* 552:54–59. doi:10.1016/j.tca.2012.11.003
37. Kan T, Strezov V, Evans TJ (2016) Lignocellulosic biomass pyrolysis: a review of product properties and effects of pyrolysis parameters. *Renew Sust Energ Rev* 57:1126–1140. doi:10.1016/j.rser.2015.12.185
38. Yang H, Yan R, Chen H et al (2007) Characteristics of hemicellulose, cellulose and lignin pyrolysis. *Fuel* 86:1781–1788. doi:10.1016/j.fuel.2006.12.013
39. Liu Q, Zhong Z, Wang S, Luo Z (2011) Interactions of biomass components during pyrolysis: a TG-FTIR study. *J Anal Appl Pyrolysis* 90:213–218. doi:10.1016/j.jaap.2010.12.009
40. Mendu V, Harman-Ware AE, Crocker M et al (2011) Identification and thermochemical analysis of high-lignin feedstocks for biofuel and biochemical production. *Biotechnol Biofuels* 4:43. doi:10.1186/1754-6834-4-43
41. Collard F-X, Blin J (2014) A review on pyrolysis of biomass constituents: mechanisms and composition of the products obtained from the conversion of cellulose, hemicelluloses and lignin. *Renew Sust Energ Rev* 38:594–608. doi:10.1016/j.rser.2014.06.013
42. Stefanidis SD, Kalogiannis KG, Iliopoulou EF et al (2014) A study of lignocellulosic biomass pyrolysis via the pyrolysis of cellulose, hemicellulose and lignin. *J Anal Appl Pyrolysis* 105:143–150. doi:10.1016/j.jaap.2013.10.013
43. Jiang G, Nowakowski DJ, Bridgwater AV (2010) A systematic study of the kinetics of lignin pyrolysis. *Thermochim Acta* 498:61–66. doi:10.1016/j.tca.2009.10.003
44. Caballero JA, Conesa JA, Font R, Marcilla A (1997) Pyrolysis kinetics of almond shells and olive stones considering their organic fractions. *J Anal Appl Pyrolysis* 42:159–175. doi:10.1016/S0165-2370(97)00015-6
45. Chen Z, Hu M, Zhu X et al (2015) Characteristics and kinetic study on pyrolysis of five lignocellulosic biomass via thermogravimetric analysis. *Bioresour Technol* 192:441–450. doi:10.1016/j.biortech.2015.05.062
46. Barneto AG, Carmona JA, Alfonso JEM, Serrano RS (2010) Simulation of the thermogravimetry analysis of three non-wood pulps. *Bioresour Technol* 101:3220–3229. doi:10.1016/j.biortech.2009.12.034
47. Branca C, Albano A, Di Blasi C (2005) Critical evaluation of global mechanisms of wood devolatilization. *Thermochim Acta* 429:133–141. doi:10.1016/j.tca.2005.02.030
48. Gani A, Naruse I (2007) Effect of cellulose and lignin content on pyrolysis and combustion characteristics for several types of biomass. *Renew Energy* 32:649–661. doi:10.1016/j.renene.2006.02.017
49. Lv D, Xu M, Liu X et al (2010) Effect of cellulose, lignin, alkali and alkaline earth metallic species on biomass pyrolysis and gasification. *Fuel Process Technol* 91:903–909. doi:10.1016/j.fuproc.2009.09.014
50. Hu S, Jess A, Xu M (2007) Kinetic study of Chinese biomass slow pyrolysis: comparison of different kinetic models. *Fuel* 86:2778–2788. doi:10.1016/j.fuel.2007.02.031
51. Sanchez-Jimenez PE, Pérez-Maqueda LA, Perejon A, Criado JM (2010) Generalized kinetic master plots for the thermal degradation of polymers following a random scission mechanism. *J Phys Chem A* 114:7868–7876. doi:10.1021/jp103171h
52. Burnham AK, Zhou X, Broadbelt LJ Critical review of the global chemical kinetics of cellulose thermal decomposition. doi: 10.1021/acs.energyfuels.5b00350